Detection of the propargyl radical at λ 3 mm*

M. Agúndez¹, N. Marcelino^{2,3}, C. Cabezas¹, R. Fuentetaja¹, B. Tercero^{2,3}, P. de Vicente³, and J. Cernicharo¹

- ¹ Instituto de Física Fundamental, CSIC, Calle Serrano 123, E-28006 Madrid, Spain e-mail: marcelino.agundez@csic.es, jose.cernicharo@csic.es
- Observatorio Astronómico Nacional, IGN, Calle Alfonso XII 3, E-28014 Madrid, Spain
- Observatorio de Yebes, IGN, Cerro de la Palera s/n, E-19141 Yebes, Guadalajara, Spain

Received; accepted

ABSTRACT

We report the detection of the propargyl radical (CH₂CCH) in the cold dark cloud TMC-1 in the λ 3 mm wavelength band. We recently discovered this species in space toward the same source at a wavelength of λ 8 mm. In those observations, various hyperfine components of the 2_{0.2}-1_{0.1} rotational transition, at 37.5 GHz, were detected using the Yebes 40m telescope. Here, we used the IRAM 30m telescope to detect ten hyperfine components of the $5_{0.5}$ - $4_{0.4}$ rotational transition, lying at 93.6 GHz. The observed frequencies differ by 0.2 MHz with respect to the predictions from available laboratory data. This difference is significant for a radioastronomical search for CH₂CCH in interstellar sources with narrow lines. We thus included the measured frequencies in a new spectroscopic analysis to provide accurate frequency predictions for the interstellar search for propargyl at mm wavelengths. Moreover, we recommend that future searches for CH_2CCH in cold interstellar clouds are carried out at $\lambda 3$ mm, rather than at $\lambda 8$ mm. The $5_{0.5}$ - $4_{0.4}$ transition is about five times more intense than the $2_{0.2}$ - $1_{0.1}$ one in TMC-1, which implies that detecting the former requires about seven times less telescope time than detecting the latter. We constrain the rotational temperature of CH₂CCH in TMC-1 to 9.9 ± 1.5 K, which indicates that the rotational levels of this species are thermalized at the gas kinetic temperature. The revised value of the column density of CH₂CCH (including ortho and para species) is $(1.0 \pm 0.2) \times 10^{14}$ cm⁻², and thus the CH₂CCH/CH₃CCH abundance ratio is revised from slightly below one to nearly one. This study opens the door for future detections of CH₂CCH in other cold interstellar clouds, making possible to further investigate the role of this very abundant hydrocarbon radical in the synthesis of

Key words. astrochemistry - line: identification - molecular processes - ISM: molecules - radio lines: ISM

We report the detection of the propargyl radical (CH₂CCH) in the recently discovered this species in space toward the same source at components of the 20,2-10,1 rotational transition, at 37.5 GHz, we IRAM 30m telescope to detect ten hyperfine components of the frequencies differ by 0.2 MHz with respect to the predictions for radioastronomical search for CH₂CCH in interstellar sources with new spectroscopic analysis to provide accurate frequency predict Moreover, we recommend that future searches for CH₂CCH in cmm. The 50,5-40,4 transition is about five times more intense than the requires about seven times less telescope time than detecting the lat to 9.9 ± 1.5 K, which indicates that the rotational levels of this syvalue of the column density of CH₂CCH (including ortho and para subundance ratio is revised from slightly below one to nearly one. To cold interstellar clouds, making possible to further investigate the large organic molecules such as aromatic rings.

Key words. astrochemistry – line: identification – molecular proceed in the foliation of th

It is not yet well understood which chemical routes are behind the formation of these aromatic cycles in cold dark clouds like TMC-1. Hydrocarbon radicals are likely key players in the synthesis of these large molecules from smaller species. How-

ever, only a few such radicals have been detected. The methylidyne radical CH and the polyacetylenic radicals C₂H, C₃H, C₄H, and even longer ones are known from long time ago. Other radicals such as C₂H₃, C₃H₃, or C₃H₅ are likely important pieces in the synthesis of large hydrocarbons but detecting them has been proven to be difficult due to different possible reasons like spectral dilution due to splitting of rotational lines into numerous fine and hyperfine components, low abundance, low dipole moment, or lack of sufficiently sensitive radioastronomical observations. We recently identified the propargyl radical (CH₂CCH) toward TMC-1 as part of the OUIJOTE line survey (Agúndez et al. 2021a). It was found that CH₂CCH is one of the most abundant radicals in TMC-1, being present at the level of its closedshell counterpart CH₃CCH. Being that abundant, the propargyl radical becomes a very attractive candidate to play an important role in the synthesis of aromatic molecules. For example, calculations indicate that the propargyl radical self reaction can lead to cyclization producing the aromatic radical phenyl radical at low temperatures (Miller & Klippenstein 2001; Zhao et al. 2021).

The radical CH₂CCH was detected in TMC-1 at λ8 mm through six hyperfine components belonging to the $2_{0.2}$ - $1_{0.1}$ rotational transition. Here we report the detection of CH₂CCH toward TMC-1 at λ 3 mm. We observed the 5_{0,5}-4_{0,4} transition in ten hyperfine components, with frequencies that differ by 0.2 MHz from previous available predictions. We thus used the observed frequencies to improve the spectroscopic parameters of CH₂CCH and provide accurate predictions to guide future astronomical searches. Moreover, the $\lambda 3$ mm line is about five times

^{*} Based on observations carried out with the Yebes 40m telescope (projects 19A003, 20A014, 20D023, and 21A011) and the IRAM 30m telescope. The 40m radiotelescope at Yebes Observatory is operated by the Spanish Geographic Institute (IGN, Ministerio de Transportes, Movilidad y Agenda Urbana). IRAM is supported by INSU/CNRS (France), MPG (Germany) and IGN (Spain).

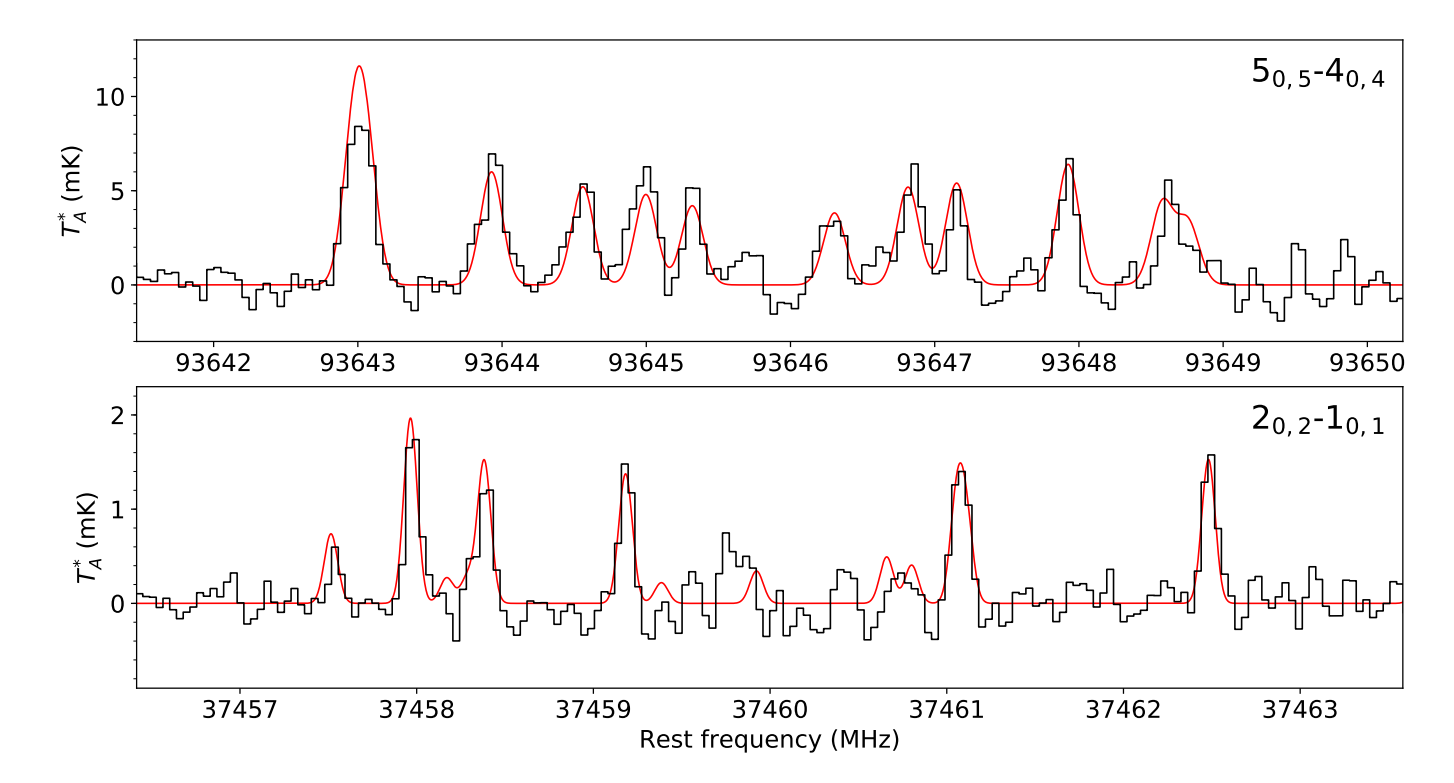


Fig. 1. Observed spectra of TMC-1 around the $2_{0.2}$ - $1_{0.1}$ and $5_{0.5}$ - $4_{0.4}$ rotational transitions of ortho CH₂CCH. The spectrum at 37.5 GHz is taken with the Yebes 40m telescope (black histogram in bottom panel) and that at 93.6 GHz is taken with the IRAM 30m telescope (black histogram in top panel). Transition quantum numbers, frequencies, and derived line parameters are given in Table 1. The synthetic spectra (red lines) were computed for a column density of ortho CH₂CCH of 7.5×10^{13} cm⁻², a rotational temperature of 9.9 K, an emission size of 40" of radius, and a linewidth of 0.72 km s⁻¹ for the $2_{0.2}$ - $1_{0.1}$ lines and of 0.57 km s⁻¹ for the $5_{0.5}$ - $4_{0.4}$ lines (see text).

more intense than the λ 8 mm one, which suggests that the search for CH₂CCH in other cold dark clouds is more favorable in the λ 3 mm wavelength band.

2. Observations

The observations of TMC-1 at $\lambda 3$ mm were carried out using the IRAM 30m telescope in September 2021. The observed position corresponds to the cyanopolyyne peak of TMC-1, α_{J2000} = $4^{h}41^{m}41.9^{s}$ and $\delta_{J2000} = +25^{\circ}41'27.0''$. The 3 mm EMIR receiver was used connected to a fast Fourier transform spectrometer, providing a spectral resolution of 48.84 kHz. We covered the spectral region around 93.6 GHz, where the $5_{0.5}$ - $4_{0.4}$ rotational transition of CH₂CCH is located. We observed two setups at slightly different central frequencies in order to check for spurious signals, line emission from the image band, and other technical artifacts. The observations were performed in the frequency-switching observing mode with a frequency throw of 18 MHz, large enough to avoid possible contamination from negative frequency-switching artifacts arising from the different hyperfine components of CH₂CCH. Pointing scans were performed on strong and nearby quasars every 1-1.5 h, with pointing errors always within 3-5". The antenna focus was checked every ~6 h at the beginning of each observing session and after sunrise. Weather conditions were between good and average for the summer period, with opacities of 0.4-0.5 at 225 GHz and amounts of precipitable water vapor ranging from 1-3 mm to 6-7 mm. The spectra were calibrated in antenna temperature, T_A^* , corrected for atmospheric attenuation and for antenna ohmic and spillover losses, using the ATM package (Cernicharo 1985; Pardo et al. 2001). The uncertainty in the calibration is estimated to be 10 %.

System temperatures varied between 100 and 140 K and the final T_A^* rms at 93.6 GHz is 1.1 mK after 31.4 h of total on-source telescope time.

The final spectra shown in Fig. 1 is obtained after averaging the data taken in September 2021 with previous spectra from our TMC-1 3 mm line survey (Marcelino et al. 2007; Cernicharo et al. 2012). At the frequency of the $5_{0.5}$ - $4_{0.4}$ transition of CH₂CCH, the observed time in the survey data is 4.0 h. Including these data has improved the final sensitivity down to 0.9 mK, resulting in a total on-source integration time of 35.4 h for each polarization (twice this value after averaging the two polarizations).

We also present a more sensitive spectrum of TMC-1 at the frequency of the 2_{0.2}-1_{0.1} transition of CH₂CCH, 37.5 GHz, with respect to that presented by Agúndez et al. (2021a). New data was gathered in several observing sessions between January and May 2021. These data are part of the on going QUIJOTE line survey that is being carried out with the Yebes 40m telescope. The line survey uses a 7 mm receiver covering the Q band, from 31.0 GHz to 50.3 GHz, with horizontal and vertical polarizations. A detailed description of the system is given by Tercero et al. (2021). Receiver temperatures in the observing sessions carried out during 2020 vary from 22 K at 32 GHz to 42 K at 50 GHz. Some power adaptation in the down-conversion chains has reduced the receiver temperatures during 2021 to 16 K at 32 GHz and 25 K at 50 GHz. The backends are $2 \times 8 \times 2.5$ GHz fast Fourier transform spectrometers with a spectral resolution of 38.15 kHz providing the whole coverage of the Q band in both polarizations. The QUIJOTE observations are performed using the frequency-switching observing mode with a frequency throw of 10 MHz in the very first observing runs, during November 2019 and February 2020, and of 8 MHz in the later ones. The

Table 1. Observed line parameters of CH₂CCH in TMC-1.

Transition ^a	$\nu_{ m calc}^{\ \ b}$	$ u_{ m obs}^{\ \ c}$	Δv^d	T_A^* peak	$\int T_A^* dv$	S/N e
	(MHz)	(MHz)	$(km s^{-1})$	(mK)	$(mK km s^{-1})$	(σ)
$2_{0,2}$ - $1_{0,1}$ $J = 3/2$ - $1/2$ $F_1 = 2$ - 1 $F = 2$ - 1	37457.515	37457.542(20)	0.55(35)	0.60	0.35(22)	4.5
$2_{0,2}-1_{0,1}$ $J = 5/2-3/2$ $F_1 = 3-2$ $F = 4-3$	37457.965	37457.981(10)	0.71(16)	1.92	1.45(27)	16.4
$2_{0,2}-1_{0,1}$ $J = 5/2-3/2$ $F_1 = 2-1$ $F = 3-2$	37458.382	37458.390(13)	0.80(27)	1.28	1.09(29)	11.6
$2_{0,2}-1_{0,1}$ $J = 5/2-3/2$ $F_1 = 3-2$ $F = 3-2$	37459.186	37459.187(10)	0.65(14)	1.58	$1.09(22)^{f}$	12.9
$2_{0,2}-1_{0,1}$ $J = 5/2-3/2$ $F_1 = 2-1$ $F = 2-1$	37461.057	27461 079(11)	0.85(15)	1.53	1.38(25) ^g	14.3
$2_{0,2}-1_{0,1}$ $J = 5/2-3/2$ $F_1 = 2-1$ $F = 2-1$	37461.111	}37461.078(11)	0.83(13)	1.33	1.38(23)	14.5
$2_{0,2}-1_{0,1}$ $J=3/2-1/2$ $F_1=2-1$ $F=3-2$	37462.481	37462.489(10)	0.76(17)	1.63	1.31(25)	14.3
$5_{0,5}$ - $4_{0,4}$ $J = 11/2$ - $9/2$ $F_1 = 6$ - 5 $F = 7$ - 6	93642.970	}93643.011(15)	0.69(11)	9.00	$6.60(93)^g$	22.3
$5_{0,5}-4_{0,4}$ $J = 11/2-9/2$ $F_1 = 5-4$ $F = 6-5$	93643.059	393043.011(13)	0.09(11)	9.00	0.00(93)	22.3
$5_{0,5}$ - $4_{0,4}$ $J = 11/2$ - $9/2$ $F_1 = 6$ - 5 $F = 6$ - 5	93643.927	93643.940(22)	0.65(18)	6.25	4.32(97)	15.1
$5_{0,5}$ - $4_{0,4}$ $J = 11/2$ - $9/2$ $F_1 = 6$ - 5 $F = 5$ - 4	93644.560	93644.557(28)	0.66(24)	4.98	3.51(99)	12.1
$5_{0,5}$ - $4_{0,4}$ $J = 11/2$ - $9/2$ $F_1 = 5$ - 4 $F = 5$ - 4	93644.997	93644.982(22)	0.65(16)	6.19	4.30(92)	15.0
$5_{0,5}$ - $4_{0,4}$ $J = 11/2$ - $9/2$ $F_1 = 5$ - 4 $F = 4$ - 3	93645.319	93645.325(18)	0.38(14)	5.76	2.34(71)	10.7
$5_{0,5}$ - $4_{0,4}$ $J = 9/2$ - $7/2$ $F_1 = 4$ - 3 $F = 4$ - 3	93646.305	93646.286(48)	0.61(30)	3.68	2.40(114)	8.6
$5_{0.5}$ - $4_{0.4}$ $J = 9/2$ - $7/2$ $F_1 = 4$ - 3 $F = 5$ - 4	93646.815	93646.849(31)	0.61(32)	5.73	3.72(136)	13.4
$5_{0,5}$ - $4_{0,4}$ $J = 9/2$ - $7/2$ $F_1 = 5$ - 4 $F = 5$ - 4	93647.152	93647.155(25)	0.35(17)	5.13	1.89(87)	9.0
$5_{0.5}$ - $4_{0.4}$ $J = 9/2$ - $7/2$ $F_1 = 5$ - 4 $F = 6$ - 5	93647.925	93647.919(24)	0.44(18)	6.36	2.99(103)	12.7
$5_{0.5}$ - $4_{0.4}$ $J = 9/2-7/2$ $F_1 = 5-4$ $F = 4-3$	93648.580	02649 649(41)	0.62(45)	1 65	2.07(1.45) 8	11.0
$5_{0,5}$ - $4_{0,4}$ $J = 9/2$ - $7/2$ $F_1 = 4$ - 3 $F = 3$ - 2	93648.750	}93648.648(41)	0.62(45)	4.65	$3.07(145)^g$	11.0

The line parameters v_{obs} , Δv , T_A^* peak, and $\int T_A^* dv$ as well as the associated errors were derived from a Gaussian fit to each line profile.

main beam efficiency of the Yebes 40m telescope varies from 0.6 at 32 GHz to 0.43 at 50 GHz. The intensity scale used in this work, antenna temperature (T_A^*) , was calibrated using two absorbers at different temperatures and the atmospheric transmission model ATM (Cernicharo 1985; Pardo et al. 2001). Calibration uncertainties were adopted to be 10 %. After including all data taken between November 2019 and May 2021, the total on-source telescope time is 238 h in each polarization (twice this value after averaging the two polarizations). The IRAM 30m and Yebes 40m data were analyzed using the GILDAS software¹.

3. Results and discussion

3.1. Improved rotational spectroscopy for CH₂CCH

The rotational spectrum of the propargyl radical has been measured in the laboratory at frequencies below 38 GHz by Tanaka et al. (1997). Due to the existence of two equivalent H nuclei, the radical has ortho/para statistics. Ortho levels have K_a even and para levels have K_a odd. The statistical ortho-to-para ratio is three. The dipole moment of CH₂CCH has been calculated by Botschwina et al. (1995) to be 0.14 D, while more recently, Küpper et al. (2002) measured a value of 0.150 ± 0.005 D, which is the value we adopt hereafter.

Our IRAM 30m data of TMC-1 show a group of lines spanning 6 MHz around 93646 MHz (see top panel in Fig. 1), which

https://cdms.astro.uni-koeln.de/

tion of CH₂CCH. The measured frequencies are systematically shifted up by 0.2 MHz with respect to the predicted frequencies in the Cologne Database for Molecular Spectroscopy (CDMS; Müller et al. 2005)². The entry in the CDMS is based on a fit to the laboratory frequencies measured by Tanaka et al. (1997). These authors measured the fine and hyperfine structure of the rotational transitions $1_{0,1}$ - $0_{0,0}$, $2_{0,2}$ - $1_{0,1}$, $2_{1,2}$ - $1_{1,1}$, and $2_{1,1}$ - $1_{1,0}$, lying at 18.7 GHz and in the 37-38 GHz range. Although the experimental accuracy is quite good, a few kilohertz, the limited range of J values covered makes that when extrapolating to the $\lambda 3$ mm wavelength band, the frequency errors could be significant for radioastronomical purposes. The CDMS quotes frequency errors of just ~ 55 kHz for the hyperfine components of the $5_{0.5}$ - $4_{0.4}$ transition, although our TMC-1 observations shows that the error is in fact as high as ~ 200 kHz. This is significant for a radioastronomical search for CH2CCH in sources with narrow lines, such as TMC-1.

we assign to the hyperfine components of the 5_{0.5}-4_{0.4} transi-

In order to obtain more accurate frequency predictions for CH_2CCH we carried out a new spectroscopic analysis using the SPFIT program (Pickett 1991) including the laboratory frequencies of Tanaka et al. (1997) and the astronomical frequencies measured in TMC-1 for the ten hyperfine components of the $5_{0.5}$ - $4_{0.4}$ transition (see derived line parameters in Table 1). The Hamiltonian used for the analysis is the same than that employed

^a Quantum numbers from the coupling scheme of Tanaka et al. (1997).

^b Calculated frequencies ν_{calc} from the combined laboratory+astronomical fit carried out in this work.

^c Observed frequencies adopting a systemic velocity of 5.83 km s⁻¹ for TMC-1 (Cernicharo et al. 2020).

 $^{^{}d} \Delta v$ is the full width at half maximum (FWHM).

^e The signal-to-noise ratio is computed as S/N = $\int T_A^* dv / [\text{rms} \times \sqrt{\Delta v \times \delta v (c/v_{\text{calc}})}]$, where c is the speed of light and δv is the spectral resolution. For the lines observed with the Yebes 40m telescope at 37.5 GHz $\delta v = 0.03815$ MHz and rms = 0.19 mK, while for the lines observed with the IRAM 30m telescope at 93.6 GHz $\delta v = 0.04884$ MHz and rms = 0.9 mK. The rest of parameters are given in the table.

^f Line overlaps with the $2_{1,2}$ - $1_{1,1}$ transition of syn- C_2H_3OH , which lies at 37459.184 MHz (see Agúndez et al. 2021b). The observed intensity is thus the sum of the CH₂CCH and the syn- C_2H_3OH lines.

^g Observed line results from a blend of two unresolved hyperfine components.

nich

http://www.iram.fr/IRAMFR/GILDAS/

Table 2. Spectroscopic parameters of CH₂CCH (all in MHz).

Parameter	Global Fit	Tanaka et al. (1997)
A	288055 a	288055
B	9523.6746(41)	9523.6775(60)
C	9206.8776(41)	9206.8805(60)
Δ_N	0.003004(72)	0.003440(63)
Δ_{NK}	0.3758(28)	0.3753(28)
Δ_K	22.62^{a}	22.62
δ_N	0.000103^{a}	0.000103
δ_K	0.1575^{a}	0.1575
$oldsymbol{arepsilon}_{aa}$	-529.386(60)	-529.386(60)
$arepsilon_{bb}$	-11.524(31)	-11.524(30)
$arepsilon_{cc}$	-0.520(31)	-0.520(30)
$a_F^{(H_a)}$	-36.322(25)	-36.323(24)
$T_{aa}^{\rm (H_a)}$	17.400(26)	17.400(24)
$T_{hh}^{(\mathrm{H_a})}$	-17.220(38)	-17.220(37)
$a_F^{(H_m)}$	-54.20(12)	-54.21(11)
$T_{aa}^{(\mathrm{H_m})}$	-14.122(20)	-14.121(19)
$T_{bb}^{(\mathrm{H_m})}$	12.88 a	12.88
rms b	6.3	7.0
N ^c	55	46

Numbers in parentheses are 3σ uncertainties in units of the last digits. H_a and H_m refer to the acetylenic and methylenic hydrogen nuclei, respectively.

Table 3. Rotational partition function (Q_r) of CH₂CCH at different temperatures.

T (IZ)	
Temperature (K)	Q_r
9.375	294.5
18.750	718.9
37.500	1959.3
75.000	5506.5
150.000	14710.5
225.000	24377.0
300.000	33479.9

by Tanaka et al. (1997) and it has the following form:

$$H = H^{rot} + H^{cd} + H^{sr} + H^{mhf} \tag{1}$$

where H^{rot} and H^{cd} contain the rotational and centrifugal distortion parameters, respectively, H^{sr} is the spin-rotation term, and H^{mhf} represents the magnetic hyperfine coupling interaction between the unpaired electron and the hydrogen nuclei. A complete description of these terms can be found in Tanaka et al. (1997). The coupling scheme used is $\mathbf{J} = \mathbf{N} + \mathbf{S}$, $\mathbf{F}_1 = \mathbf{J} + \mathbf{I}_1$, and $\mathbf{F} = \mathbf{F}_1 + \mathbf{I}_2$, where $\mathbf{I}_1 = \mathbf{I}(\mathbf{H}_a)$ and $\mathbf{I}_2 = \mathbf{I}(\mathbf{H}_{m1}) + \mathbf{I}(\mathbf{H}_{m2})$. The radical CH₂CCH has two equivalent H nuclei, the methylenic ones, and the hyperfine interaction term H^{mhf} is thus written explicitly as a two spin system:

$$H^{mhf} = a_F^{(\mathbf{H}_{a})} \cdot \mathbf{S} \cdot \mathbf{I}_1 + \mathbf{I}_1 \cdot \mathbf{T}^{(\mathbf{H}_{a})} \cdot \mathbf{S} + a_F^{(\mathbf{H}_{m1}, \mathbf{H}_{m2})} \cdot \mathbf{S} \cdot \mathbf{I}_2 + \mathbf{I}_2 \cdot \mathbf{T}^{(\mathbf{H}_{m1}, \mathbf{H}_{m2})} \cdot \mathbf{S}$$
(2)

where $a_F^{(\mathrm{H_a})}$ and $\mathbf{T}^{(\mathrm{H_a})}$ stand for the Fermi contact constant and the dipole-dipole interaction tensor for the acetylenic hydrogen nucleus, respectively, and $a_F^{(\mathrm{H_{m1},H_{m2})}}$ and $\mathbf{T}^{(\mathrm{H_{m1},H_{m2})}}$ are averages of the coupling constants for the two methylenic hydrogen nuclei that are equivalent. In this manner, each energy level is denoted by six quantum numbers: N, K_a , K_c , J, F_1 , and F.

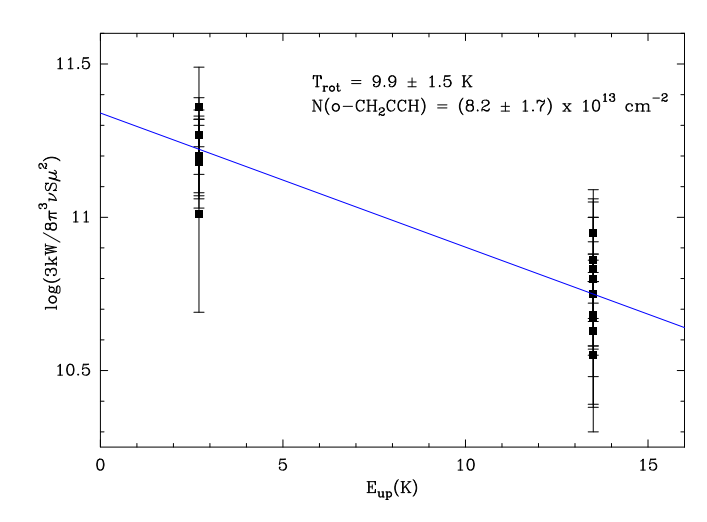


Fig. 2. Rotation diagram of ortho CH₂CCH in TMC-1.

The results obtained from the fit are shown in Table 2, where they are compared with those reported by Tanaka et al. (1997). As expected, the new derived parameters for CH₂CCH are almost identical to those reported before. The inclusion of the $5_{0.5}$ - $4_{0,4}$ transition in the fit only affects the rotational constants B and C and the distortion constants Δ_N and Δ_{NK} . For B, C and Δ_{NK} the differences are smaller than the 3σ uncertainties. However, for the Δ_N distortion constant the difference is much larger, as expected, due to the inclusion of rotational transitions with higher quantum number N. We used the spectroscopic parameters obtained in this work for CH₂CCH to obtain accurate frequency predictions at mm wavelengths. The catalog file with the predicted frequencies and the calculated intensities at 300 K is provided at the CDS. The intensities are calculated adopting a dipole moment of 0.150 D, the experimental value measured by Küpper et al. (2002). The rotational partition functions used in these predictions are listed at different temperatures in Table 3. The rotational partition function was calculated considering a maximum value of 30 for the quantum number N.

3.2. Excitation and abundance of CH₂CCH in TMC-1, and guidance for further searches

We also present the observed spectrum of TMC-1 at the frequency of the $2_{0,2}$ - $1_{0,1}$ transition of CH₂CCH (see bottom panel in Fig. 1). This spectrum is more sensitive than that presented in Agúndez et al. (2021a) because it includes additional observations taken with the Yebes 40m telescope. The rms noise level has decreased from 0.30 mK to 0.19 mK, per 38.15 kHz channel. As a consequence, the CH₂CCH lines are now more clearly detected. The new line parameters derived for the six hyperfine components of the $2_{0,2}$ - $1_{0,1}$ transition of CH₂CCH are given in Table 1.

As can be seen in Fig. 1, the strongest hyperfine component of the $5_{0.5}$ - $4_{0.4}$ transition is about five times more intense than the strongest component of the $2_{0.2}$ - $1_{0.1}$. This is consistent with the rotational temperature of CH₂CCH being close to the gas kinetic temperature of TMC-1, ~ 10 K (Fehér et al. 2016). At this temperature, the $5_{0.5}$ rotational level, with an energy of ~ 13.5 K, is expected to be more populated than the $2_{0.2}$ level, which has an energy of ~ 2.7 K. In addition, the Einstein coefficient of spontaneous emission is about 20 times larger for the $5_{0.5}$ - $4_{0.4}$ transition than for the $2_{0.2}$ - $1_{0.1}$. These facts make the $5_{0.5}$ - $4_{0.4}$ transition at 93.6 GHz more favorable for detection than the $2_{0.2}$ - $1_{0.1}$ transition th

^a Parameter fixed to the value reported by Tanaka et al. (1997).

^b Standard deviation of the fit in kHz.

^c Number of lines included in the fit.

sition at 37.5 GHz. Indeed, if we assume typical values for the system temperatures, $T_{\rm sys} = 40$ K at 37.5 GHz with the Yebes 40m telescope and $T_{\rm sys} = 120$ K at 93.6 GHz with the IRAM 30m telescope, and we keep in mind that the line at 93.6 GHz is five times more intense than the 37.5 GHz line, the radiometer equation tells us that in order to detect the two lines with the same signal-to-noise ratio (S/N) one must invest ~ 7 times more integration time at the Yebes 40m telescope than with IRAM 30m telescope. The fact that in our data the $2_{0,2}$ - $1_{0,1}$ transition is detected with similar or even higher S/N than the 5_{0,5}-4_{0,4} transition (see Table 1) is a consequence of the much longer integration time invested with the Yebes 40m telescope (238 h) compared to that employed for the IRAM 30m spectrum (35.4 h). In summary, the rotational transitions in the λ 3 mm wavelength band, in particular the 5_{0,5}-4_{0,4} at 93.6 GHz (see below), are the most favorable for detection and should be the target in future searches for CH₂CCH in cold dark clouds.

The availability of two rotational transitions with different upper level energies allows us to constrain the rotational temperature of the propargyl radical in TMC-1. We built a rotation diagram using the velocity-integrated intensities given in Table 1 and we derive a rotational temperature of 9.9 ± 1.5 K (see Fig. 2). We therefore confirm the assumption made by Agúndez et al. (2021a) that the rotational levels of CH₂CCH are thermalized at the gas kinetic temperature of TMC-1, ~10 K (Fehér et al. 2016). This fact is expected based on the low dipole moment of CH₂CCH (0.150 D; Küpper et al. 2002), which implies low critical densities, probably a few 10² cm⁻³, i.e., well below the volume density of H₂ in TMC-1, a few 10⁴ cm⁻³ (Pratap et al. 1997; Cordiner et al. 2013). The column density derived from the rotation diagram for ortho CH2CCH is $(8.2\pm1.7)\times10^{13}$ cm⁻². A more precise determination of the column density can be obtained by fitting the observed spectra with synthetic spectra calculated under local thermodynamic equilibrium. For this calculation we adopted a rotational temperature of 9.9 K, as derived from the rotation diagram, a full width at half maximum (FWHM) of 0.72 km s^{-1} for the $2_{0,2}\text{-}1_{0,1}$ lines and 0.57 km s^{-1} for the $5_{0,5}$ - $4_{0,4}$ lines, which are the arithmetic mean of the values derived for the hyperfine components of each transition (see Table 1), and assumed that the emission is distributed in the sky as a circle with a radius of 40", as observed for various hydrocarbons in TMC-1 (Fossé et al. 2001). The observed spectra at 37.5 GHz and 93.6 GHz are well reproduced adopting a column density of $7.5 \times 10^{13} \text{ cm}^{-2}$ (see Fig. 1). Assuming an ortho-to-para ratio of three, the column density of CH₂CCH (including ortho and para) in TMC-1 is $(1.0\pm0.2)\times10^{14}$ cm⁻², which is slightly higher than the value derived previously by Agúndez et al. (2021a). The column density of the closed-shell counterpart CH₃CCH in TMC-1 is $(1.1-1.3) \times 10^{14}$ cm⁻² (Gratier et al. 2016; Cabezas et al. 2021). Therefore, in this study we confirm that the propargyl radical is thermalized to the gas kinetic temperature of TMC-1 and revise the abundance ratio CH₂CCH/CH₃CCH from slightly below one to nearly one.

There are other rotational transitions of CH₂CCH that lie in the frequency range covered by our Yebes 40m and IRAM 30m data. The two other transitions of ortho CH₂CCH that fall in the λ 3 mm band, the $4_{0.4}$ - $3_{0.3}$ at 74.9 GHz and the $6_{0.6}$ - $5_{0.5}$ at 112.3 GHz, are predicted to be as intense as the $5_{0.5}$ - $4_{0.4}$. However, our data at these frequencies are not as sensitive as at 93.6 GHz, and thus the strongest hyperfine components of each transition are only marginally detected. System temperatures at 74.9 GHz and 112.3 GHz are higher than at 93.6 GHz, making the 5_{0,5}-4_{0,4} transition the most favorable for detection. There are also several lines of para CH₂CCH accessible. Two of them, the $2_{1,2}$ - $1_{1,1}$ at

37.2 GHz and the $2_{1,1}$ - $1_{1,0}$ at 37.8 GHz, lie in the Q band and are covered by our Yebes 40m line survey, while two other transitions, the $5_{1,5}$ - $4_{1,4}$ at 92.8 GHz and the $5_{1,4}$ - $4_{1,3}$ at 94.4 GHz, lie in the $\lambda 3$ mm band and are covered by our IRAM 30m telescope data. These lines are predicted to be less intense than those of ortho CH₂CCH, and thus are more difficult to detect. In our data only the strongest hyperfine components of the $5_{1.5}$ - $4_{1.4}$ and $5_{1.4}$ - $4_{1.3}$ transitions are barely visible. The S/N is however low and we have thus not attempted to fit them.

4. Conclusions

We detected the 5_{0,5}-4_{0,4} transition of ortho CH₂CCH in TMC-1 using the IRAM 30m telescope. The measured frequencies for ten hyperfine components of this transition are 0.2 MHz higher than the frequency predictions available in the CDMS catalog, a difference which is significant for radioastronomical purposes. We carried out a new spectroscopic analysis of the rotational spectrum of CH₂CCH in order to provide accurate frequencies at mm wavelengths. The intensity of the $5_{0,5}$ - $4_{0,4}$ transition, lying at 93.6 GHz, is ~ 5 times higher in TMC-1 than the $2_{0.2}$ -1_{0,1} previously observed by Agúndez et al. (2021a) using the Yebes 40m telescope. We conclude that a search for CH₂CCH in other cold interstellar sources should be carried out in the $\lambda 3$ mm band, rather than at $\lambda 8$ mm, where the telescope time investment is estimated to be about seven times cheaper. The rotational temperature of CH₂CCH in TMC-1 is constrained to 9.9 ± 1.5 K, i.e., equal to the gas kinetic temperature, and the derived value of the column density is $(1.0 \pm 0.2) \times 10^{14}$ cm⁻², which makes CH₂CCH one of the most abundant hydrocarbon radicals in TMC-1.

Acknowledgements. We acknowledge funding support from Spanish Ministerio de Ciencia e Innovación through grants PID2019-106110GB-I00, PID2019-107115GB-C21, and PID2019-106235GB-I00 and from the European Research Council (ERC Grant 610256: NANOCOSMOS). M.A. also acknowledges funding support from the Ramón y Cajal programme of Spanish Ministerio de Ciencia e Innovación (grant RyC-2014-16277). We thank the referee for a careful reading of the manuscript and for useful comments.

References

49, 1683

Agúndez, M., Cabezas, C., Tercero, B., et al. 2021a, A&A, 647, L10 Agúndez, M., Marcelino, N., Tercero, B., et al. 2021b, A&A, 649, L4 Botschwina, P., Oswald, R., Flügge, J., & Horn, M. 1995, Z. Phys. Chem., 188, Burkhardt, A. M., Lee, K. L. K., Changala, P. B., et al. 2021, ApJ, 913, L18 Cabezas, C., Endo, Y., Roueff, E., et al. 2021, A&A, 646, L1 Cernicharo, J. 1985, IRAM Internal Report 52 Cernicharo, J., Marcelino, N., Roueff, E., et al. 2012, ApJ, 759, L43 Cernicharo, J., Marcelino, N., Agúndez, M., et al. 2012, ApJ, 759, L43 Cernicharo, J., Marcelino, N., Agúndez, M., et al. 2021a, A&A, 647, L2 Cernicharo, J., Agúndez, M., Cabezas, C., et al. 2021a, A&A, 647, L3 Cernicharo, J., Agúndez, M., Cabezas, C., et al. 2021b, A&A, 649, L15 Cernicharo, J., Agúndez, M., Kaiser, R. I., et al. 2021c, A&A, 649, L15 Cernicharo, J., Agúndez, M., Kaiser, R. I., et al. 2021d, A&A, 655, L1 Cordiner, M. A., Buckle, J. V., Wirström, E. S., et al. 2013, ApJ, 770, 48 Fehér, O., Tóth, L. V., Ward-Thompson, D., et al. 2016, A&A, 590, A75 Fossé, D., Cernicharo, J., Gerin, M., & Cox, P. 2001, ApJ, 552, 168 Gratier, P., Majumdar, L., Ohishi, M., et al. 2016, ApJS, 225, 25 Küpper, J., Merritt, J. M., & Miller, R. E. 2002, J. Chem. Phys., 117, 647 Marcelino, N., Cernicharo, J., Agúndez, M., et al. 2007, ApJ, 665, L127 McGuire, B. A., Burkhardt, A. M., Kalenskii, S., et al. 2018, Science, 359, 202 McGuire, B. A., Burkhardt, A. M., Kalenskii, S., et al. 2019, Science, 371, McGuire, B. A., Burkhardt, A. M., Loomis, R. A., et al. 2020, ApJ, 900, L10 McGuire, B. A., Loomis, R. A., Burkhardt, A. M., Loomis, R. A., et al. 2021, Science, 371, McGuire, B. A., Loomis, R. A., Burkhardt, A. M., et al., 2021, Science, 371, 1265 Miller, J. A. & Klippenstein, S. J. 2001, J. Phys. Chem. A, 105, 7254 Müller, H. S. P., Schlöder, F., Stutzki, J., & Winnewisser, G. 2005, J. Mol. Struct.,

Pickett, H. M. 1991, J. Mol. Spectr., 148, 371 Pardo, J. R., Cernicharo, J., & Serabyn, E. 2001, IEEE Trans. Antennas Propag.,

49, 1683 Pratap, P., Dickens, J. E., Snell, R. L., et al. 1997, ApJ, 486, 862 Tanaka, K., Sumiyoshi, Y., Ohshima, Y., et al. 1997, J. Chem. Phys., 107, 2728 Tercero, F., López-Pérez, J. A., Gallego, et al. 2021, A&A, 645, A37 Zhao, L., Lu, W., Ahmed, M., et al. 2021, Sci. Adv., 7, eabf0360